PAPER

Interacting filamentary eruptions in magnetised plasmas

IOP Publishing Plasma Physics and Controlled Fusion
Plasma Phys. Control. Fusion **57** (2015) 125010 (5pp) doi:10.1088/0741-3335/57/12/125010

Interacting filamentary eruptions in magnetised plasmas

S A Henneberg[1], S C Cowley[2,3] and H R Wilson[1]

[1] York Plasma Institute, Department of Physics, University of York, Heslington, York, YO10 5DD, UK
[2] CCFE, Culham Science Centre, Abingdon, Oxfordshire, OX14 3DB, UK
[3] Department of Physics, Imperial College, Prince Consort Road, London SW7 2BZ, UK

E-mail: Sophia.Henneberg@york.ac.uk

Received 14 May 2015, revised 24 August 2015
Accepted for publication 29 September 2015
Published 3 November 2015

Abstract

The interaction between multiple filamentary plasma eruptions is investigated by modelling the non-linear ideal MHD ballooning mode envelope equation with a mixed Eulerian and Lagrangian characterisation of the boundary conditions. The study of multiple plasma filaments is performed in a specific slab equilibrium susceptible to Rayleigh–Taylor instabilities. If the unstable system is initiated with three equal sized filaments, they erupt at the same rate, independently of each other, even in the non-linear regime. However, if one is initiated very slightly larger than the other two it causes a down-draft as it erupts upwards, which suppresses the smaller filaments. This suggests that those filaments which first enter the non-linear regime will dominate the plasma eruption dynamics.

Keywords: ELM, ideal MHD, ballooning, eruptions, filaments, filamentary, non-linear

(Some figures may appear in colour only in the online journal)

1. Introduction

Explosive events occur in a wide variety of magnetically confined plasmas and are typically associated with filamentary structures. Edge-localised modes (ELMs) [1–3] and solar flares [4], are just two examples of such explosive instabilities for laboratory and natural plasmas, respectively. Both systems initially evolve slowly until a certain threshold condition is reached, at which point their behaviour becomes rapid. This process is a feature of the non-linear ideal Magnetohydrodynamics (MHD) equations, which have been reduced using ballooning mode assumptions that exploit the filamentary nature of these eruptions [5–9] and explosive events have also been observed in two-fluid simulations (e.g. [10, 11]). We will argue that our main results are quite generic, independent of geometry and drive mechanism. We therefore demonstrate the essential physics with the relatively simple slab Rayleigh–Taylor-model, employed in [6]. We extend that calculation to derive the system with Eulerian boundary conditions, as employed in [12]. Previous investigations of this non-linear ballooning model studied the evolution of single, isolated filaments in time and space. In a real plasma system it is more likely that several filaments will erupt, and interact—ELMs are a classic example [13]. This motivates our study to determine how the interaction of filaments affects their evolution, extending the studies of [14].

2. Theoretical model

We derive the non-linear equation for perturbations to a slab Rayleigh–Taylor model equilibrium using mixed Eulerian and Lagrangian boundary conditions. We adopt a simple one dimensional magnetised plasma slab which is defined by a magnetic field $\boldsymbol{B_0} = B_0(x)\,\hat{\boldsymbol{z}}$, the pressure $p_0 = p_0(x)$, the density $\rho_0 = \rho_0(x)$ and the gravitational acceleration $\boldsymbol{g} = -g\,\hat{\boldsymbol{x}}$ where the subscript '0' indicates equilibrium quantities. We apply a standard Cartesian coordinates system, where x measures the vertical height above a reference plane, and the y-z plane defines flux surfaces.

Our starting point is the ideal MHD momentum equation with an additional kinematic, scalar viscosity term that is included to provide simple viscous dissipation [15]:

$$\rho\left(\frac{\partial \boldsymbol{v}}{\partial t} + \boldsymbol{v}\cdot\boldsymbol{\nabla}\boldsymbol{v}\right) = -\boldsymbol{\nabla}\left(p + \frac{B^2}{2}\right) + \boldsymbol{B}\cdot\boldsymbol{\nabla}\boldsymbol{B} - \rho g\hat{\boldsymbol{x}} + \nu\rho\boldsymbol{\nabla}^2\boldsymbol{v}.$$

where $\boldsymbol{v}$ is the velocity of a displaced fluid element and ν is the viscosity. We choose to perform the calculation in Lagrangian variables. In this approach all perturbed quantities can be expressed in terms of the displacement $\boldsymbol{\xi}$ of a fluid element. The position vector of this fluid element, $\boldsymbol{r}(t)$, is related to its initial position vector, $\boldsymbol{r}_0$, through $\boldsymbol{r}(t) = \boldsymbol{r}_0 + \boldsymbol{\xi}(\boldsymbol{r}_0, t)$, so that the components of the Jacobian matrix J_{ij} are $J_{ij} = \delta_{ij} + \frac{\partial \xi_j}{\partial x_{0i}}$ where x_{0i} are the components of $\boldsymbol{r}_0$. The Jacobian J is the determinant of the Jacobian matrix J_{ij}. We choose line-tied boundary conditions at the walls where $z = 0$ and $z = L$ so that $\xi_x = 0$ and $J = 1$ there, corresponding to unperturbed density and pressure. Periodic boundary conditions are adopted in the y-direction. We assume that the thermal conduction along the field lines is fast so they are isothermal. This implies that the ratio of specific heats, γ, is equal to one. The system is Rayleigh–Taylor unstable to perturbations if the density gradient exceeds a critical value. We identify a parameter $\Gamma(x_0)$, which represents the difference between the density gradient drive and the stabilising effects of the field line bending. We introduce a dummy large parameter n which characterises the ratio of the system size to the filament width in the y-direction. We expand in $n^{-1/2}$close to marginal stability, such that Γ is order $n^{-1/2}$ in the (localised) region of the perturbation. Thus $\frac{\partial}{\partial t} \sim \mathcal{O}(n^{-1/2})$. Assuming we are early in the non-linear phase, the spatial derivatives as well as the order of the Lagrangian displacement is set by the geometry of the linear ballooning mode [9]: $k_y \sim \frac{\partial}{\partial y_0} \sim \mathcal{O}(n)$, $\frac{\partial}{\partial x_0} \sim \mathcal{O}(n^{+1/2})$ and $\frac{\partial}{\partial z_0} \sim \mathcal{O}(1)$. Expanding the components of $\boldsymbol{\xi} = \xi_x \hat{\boldsymbol{x}} + \xi_y \hat{\boldsymbol{y}} + \xi_z \hat{\boldsymbol{z}}$ and the Jacobian J in powers of $n^{-1/2}$ we anticipate: $\xi_x = \sum_{i=2}^{\infty} n^{-i/2} \xi_x^{(i/2)}$, $\xi_y = \sum_{i=3}^{\infty} n^{-i/2} \xi_y^{(i/2)}$, $\xi_z = \sum_{i=2}^{\infty} n^{-i/2} \xi_z^{(i/2)}$ and $J = 1 + \sum_{i=1}^{\infty} n^{-i/2} J^{(i/2)}$. The viscosity is treated as small $\nu \sim \mathcal{O}(n^{-5/2})$ so that it only enters in our envelope equation for ξ_x. With these results the ideal MHD momentum equation is:

$$\frac{\rho_0}{J}(\boldsymbol{\nabla}_0 \boldsymbol{r}) \cdot \frac{\partial^2 \boldsymbol{\xi}}{\partial t^2} = -\boldsymbol{\nabla}_0 \left[\frac{p_0}{J} + \frac{|(\boldsymbol{B}_0 \cdot \boldsymbol{\nabla}_0 \boldsymbol{r})|^2}{2J^2} \right] + \nu \nabla_0^2 \frac{\partial \boldsymbol{\xi}}{\partial t} + (\boldsymbol{\nabla}_0 \boldsymbol{r}) \cdot \left[\frac{1}{J} (\boldsymbol{B}_0 \cdot \boldsymbol{\nabla}_0) \left(\frac{1}{J} (\boldsymbol{B}_0 \cdot \boldsymbol{\nabla}_0 \boldsymbol{r}) \right) + \frac{\rho_0}{J} \mathbf{g} \right]. \quad (1)$$

The full calculation involves expanding in $n^{-1/2}$ and follows that developed in [5, 6]. Normalising lengths to L_ρ, time to $\sqrt{\frac{L_\rho}{g}}$ and magnetic field to $\sqrt{2g\overline{\rho}_0 L_\rho}$, with the maximum density $\overline{\rho}_0$, we find:

$$C_0 \frac{\partial^2 \xi}{\partial t^2} = \Gamma_0^2(x_0)\xi + C_2 \frac{\partial^2 u}{\partial x_0^2} + C_3 \xi \frac{\partial^2 \overline{\xi^2}}{\partial x_0^2} + C_4(\xi^2 - \overline{\xi^2}) + \nu \frac{\partial^2}{\partial y_0^2} \frac{\partial \xi}{\partial t}. \quad (2)$$

Here we have introduced the 'envelope function' $\xi(x_0, y_0, t)$, defined such that $\xi_x(x_0, y_0, z_0) = \xi(x_0, y_0, t) \sin\left(\frac{\pi z}{L}\right)$ describes the vertical displacement along the field line. $\overline{\xi^2}$ is the y_0 average of the squared displacement, ξ^2 and $\frac{\partial^2 u}{\partial y_0^2} = \xi$. An important term that we shall return to later is the one involving C_4. The $\overline{\xi^2}$ piece ensures $\bar{\xi} = 0$, which is required because of the leading order result that the plasma is incompressible. The local linear growth rate Γ_0 is given by [12]:

$$\Gamma_0^2(x_0) = -\frac{B_0^2 \pi^2}{\rho_0 L^2} + \frac{\rho_0 g^2}{p_0} + \frac{g}{\rho_0} \frac{\mathrm{d}\rho_0}{\mathrm{d}x_0}.$$

where the first term is due to field line bending and is stabilising, the second term is the Parker instability drive and the third term is the Rayleigh–Taylor instability drive. In a toroidal plasma, these two drives would be replaced by the curvature drive of ballooning modes. The expressions for the remaining coefficients for our slab geometry can be found in [12]. It is worth noting that (with the exception of inertia) the structure of equation (2) is independent of geometry, which only influences the values of the coefficients.

To obtain results for a specific situation we choose the equilibrium density and magnetic field to be given by $\rho(x_0) = \frac{\overline{\rho}}{\cosh^2\left[\frac{x_0 - x_\rho}{L_\rho}\right]}$ and $B_0^2(x_0) = \overline{B}_1^2 - \frac{\overline{B}_2^2}{\cosh^2\left[\frac{x_0 - x_B}{L_\rho}\right]}$. The overlines indicate constants, x_ρ is the height of the maximum density and x_B is the height of the minimum field. Neglecting flows and curvature, the equilibrium equation derived from the force balance equation (1) can be expressed as $\frac{\partial}{\partial x_0}\left(p_0 + \frac{B_0^2}{2}\right) = -g\rho_0$. This provides the equilibrium pressure profile: $p_0(x_0) = \overline{p}_0 - \frac{B_0^2}{2} - g\overline{\rho}_0 L_\rho \tanh\left[\frac{x_0 - x_\rho}{L_\rho}\right]$. We now consider a specific equilibrium with a large pressure to ensure that the Rayleigh–Taylor drive dominates over the Parker drive: $\frac{x_\rho}{L_\rho} = 2$, $\frac{x_B}{L_\rho} = 0.8$, $\frac{\overline{B}_1^2}{2g\overline{\rho}_0} \frac{L_\rho}{L^2} = 0.078\,34$, $\frac{\overline{B}_2^2}{2g\overline{\rho}_0} \frac{L_\rho}{L^2} = 0.047\,01$ and $\nu = 10^{-10}$. With these parameters our equilibrium is close to marginal stability, with Γ^2 of order n^{-1}, as discussed above. With the definitions of the coefficients provided in [12] we obtain: $C_0 = 0.248$, $C_2 = -0.352$, $C_3 = 0.044$, $C_4 = 0.216$. We expand $\Gamma^2(x_0)$ about the position where it is a maximum, $x_{\max}$, i.e. $\Gamma^2(x_0) \approx \Gamma_0^2(x_{\max}) - \left|\frac{\mathrm{d}^2\Gamma_0^2}{\mathrm{d}x_0^2}\right| \left(\frac{(x_0 - x_{\max})^2}{2}\right) \equiv C_1\left[1 - \frac{(x_0 - x_{\max})^2}{\Delta^2}\right]$ where $C_1 = 1.9 \times 10^{-4}$, $x_{\max} = 1.1118$ and $\Delta = 0.017$ characterises the region over which $\Gamma^2 > 0$ (local instability). A linear stability analysis provides the following eigenmode structure: $\xi(x_0, y_0, t = 0) = h \cos(n y_0) \mathrm{e}^{-\sigma x^2}$ where $\sigma = \frac{n}{2\Delta}\sqrt{\frac{C_1}{|C_2|}}$ and a linear growth rate $\gamma = -\frac{n^2 \nu}{2C_0} + \sqrt{\frac{C_1}{C_0} - \frac{\sqrt{C_1\,|\,C_2|}}{C_0 n \Delta} + \frac{n^4 \nu^2}{4C_0^2}}$; h is an arbitrary constant.

To explore the non-linear evolution predicted by equation (2) we initialise the system at $t = 0$ with the linear eigenmode and evolve in time. We wish to explore how filaments of different heights evolve in time. We therefore initialise the system with a superposition of two linear eigenmodes, with $n = n_1$ and $n = n_2$:

$$\xi_{\text{init}} = h_1 \cos(n_1 y_0)\, \mathrm{e}^{(-\sigma_1 x_0^2 + \gamma_1 t)} + h_2 \cos(n_2 y_0)\, \mathrm{e}^{(-\sigma_2 x_0^2 + \gamma_2 t)}.$$

We select $n_2 = 3n_1$. This provides a perturbation which repeats every three oscillations in the y_0-direction. Thus, our

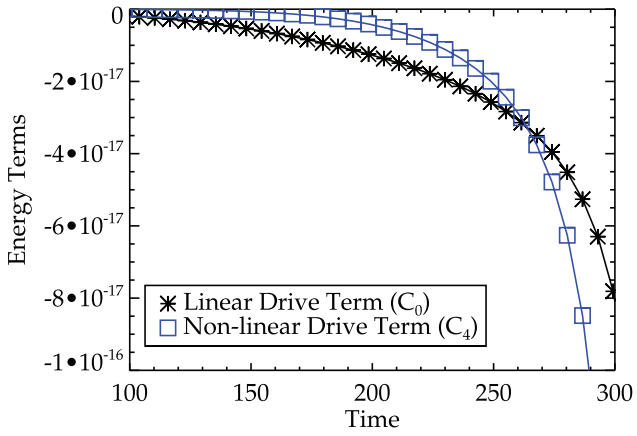

Figure 1. The two dominant drive terms of the energy equation (3) are shown. When the quadratic non-linear drive term (C_4; blue, □-symbols) intersects with the linear drive term (C_0; black, *-symbols) we assume that the non-linear dynamics start to dominate the evolution of the filaments.

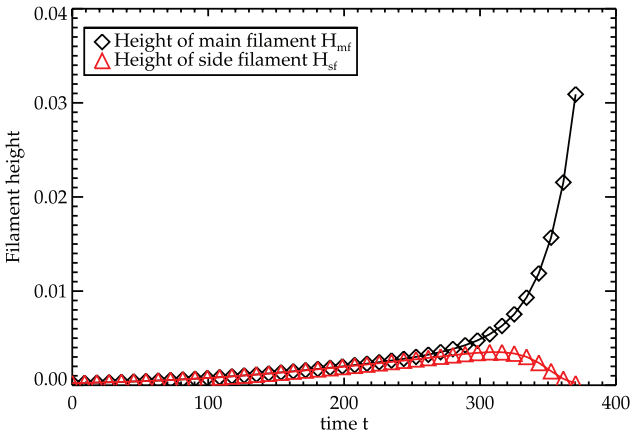

Figure 2. The normalised height at $x_0 = x_{\max}$ of the main filament $H_{\rm mf}$ (black, ◇-symbol) and the normalised height of the side filament $H_{\rm sf}$ (red, △-symbol) versus time where the heights are shifted by the minimum value of ξ at each time.

simulation domain in this direction needs to contain only three oscillations, or filaments. The results remain qualitatively the same for more filaments with different relative heights (e.g. setting $n_2 = 5n_1$ and simulating five filaments). If we take $h_1 = 0$, all three filaments will initially have the same amplitude (i.e. h_2). By introducing a small amount of h_1, we can enhance the initial amplitude of the central filament compared to the two side filaments. Provided n is large, the results do not depend strongly on the value chosen. We select $n_1 = 2600$ and $n_2 = 7800$ which have linear growth rates $\gamma_1 = 0.0033$ and $\gamma_2 = 0.0136$ respectively. Note that our choice for n provides $\gamma_2 > \gamma_1$, which ensures that the linear evolution reinforces the three filaments; therefore any deviation from this must be a non-linear effect.

We initiate our perturbation with $h_2 = 50\,h_1$ which ensures the filaments are initially very close in amplitude, but the central one penetrates slightly further than the two side filaments.

3. The evolution of multiple filaments

As the perturbation evolves, the energy is dissipated by the viscosity according to

$$2\frac{\mathrm{d}E}{\mathrm{d}t} = \frac{\mathrm{d}}{\mathrm{d}t}\int \mathrm{d}V\Bigg[C_0\left(\frac{\partial\xi}{\partial t}\right)^2 - \Gamma^2\xi^2 + C_2\left(\frac{\partial u}{\partial x_0}\right)^2 + \frac{1}{2}\,C_3\left(\frac{\partial\overline{\xi^2}}{\partial x_0}\right)^2 - \frac{2}{3}\,C_4\xi^3\Bigg] = -2\nu\int \mathrm{d}V\left(\frac{\partial^2\xi}{\partial t\partial y_0}\right)^2 \tag{3}$$

where $\int \mathrm{d}V = \int \mathrm{d}x_0\,\mathrm{d}y_0 L_z$ is a volume integral. The dominant terms are those involving C_0 and C_4 which arise from the inertia and the quadratic non-linearity of equation (2), respectively. Figure 1 shows their evolution. We estimate that the non-linear regime starts when the energy of the quadratic non-linear drive term overtakes the energy of the linear drive term, which is taking place at around $t = 260$. After this time, the behaviour of a filament approaches a finite time singularity $\xi \sim (t_0 - t)^{-\alpha}$, where α is positive [6, 7]. We can fit this asymptotic form to the amplitude of the main central filament to determine $\xi_{\rm mf} \sim (t_0 - t)^{-2.81}$. This is somewhat faster than our earlier simulations with a single, isolated filament where we found $\xi \sim (t_0 - t)^{-2.52}$ [12] (equivalent to taking $h_1 = 0$). Thus, simply enhancing one filament relative to the others by even a small amount has a significant impact on its subsequent non-linear evolution. To explore this further, we plot in figure 2 the height of the main filament above the 'ground level'. We see that the main filament accelerates continuously throughout the simulation. To understand what we mean by the 'ground level', we note that in the non-linear regime, ξ is negative and roughly constant over much of the region away from the three filaments along $x_0 = x_{\max}$ [6]. This effectively reduces the 'ground level' compared to the initial equilibrium. Thus we define $H_{\rm mf}(t) = \xi(x_0 = x_{\max}, y = 0.0, t) - \min(\xi(x_{\max}, y, t))$. We now consider the height of the side filaments ($H_{\rm sf}$ is defined in the same way) which, recall, were initiated with a height just 1.5% less than that of the main, central filament. While the side filaments grow with the main filament in the linear phase (at the linear growth rate) their growth rate reduces as they enter the non-linear regime (at $t \approx 260$), and ultimately they are completely suppressed (beyond $t \approx 370$), see figure 2. Figure 3 shows a contour plot of the flux surfaces at a later time (i.e. $t = 370$). We see that the side filaments each form a double peak away from the most unstable $x_0 = x_{\max}$ and are much smaller than the main one. Figure 4 shows how this double peak structure develops through the non-linear regime—the motion of the fluid element reverses direction at the position of maximum drive $x_0 = x_{\max}$ leaving two peaks either side.

The evolution of the ratio of the heights of the side and main filaments is shown in figure 5. During the linear phase this ratio is close to 1, as expected, but by the time overtaking occurs at $t \approx 370$ the side filaments have negligible amplitude. To compare the solution of the combined modes with the sum of the two individual mode solution we define $\Delta\xi = \xi_{n_1+n_2} - (\xi_{n_1} + \xi_{n_2})$. Here $\xi_{n_1+n_2}$ is the displacement developed from the interaction of the two modes and ξ_{n_1} and ξ_{n_2} are the solutions from two separate non-linear simulations

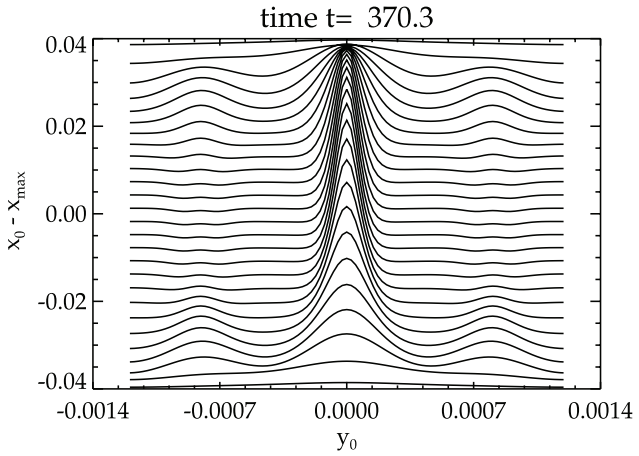

Figure 3. The flux surfaces in the x–y plane at $z = L/2$ (half way between the plates) at a time $t = 370$, which is deep in the non-linear regime, just as the perturbed flux surfaces are about to overtake each other. The two side filaments are much smaller than the main central filament.

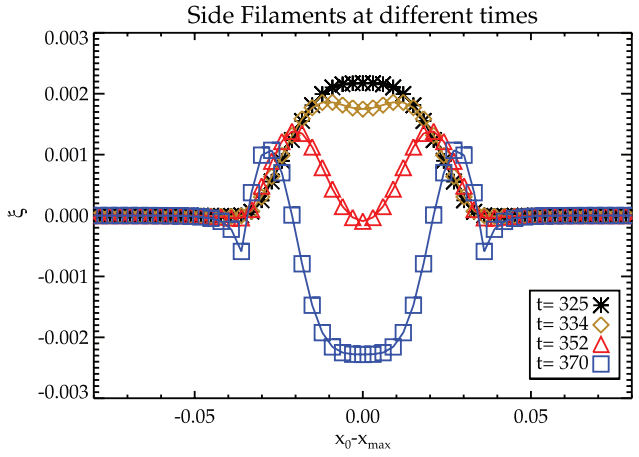

Figure 4. Evolution of a side filament versus x_0 in the non-linear regime at $y_0 \approx \pm 0.0008$. The height is mainly reduced at the centre.

for each $n = n_1$ and $n = n_2$. The plasma is in a linear regime at the beginning of the simulation as we start from close to marginal stability with a weak linear growth rate. We introduce the interaction index $p_i = \frac{\Delta\xi}{\xi_{n_1+n_2}}$ for the main filament, which characterises the fraction of the main filament height which is due to the coupling to the side filaments. In the linear phase p_i is expected to be zero, as shown in figure 5. However, deep in the non-linear regime, at $t = 370$, the height of the main filament is mostly (over 80%) due to the interaction with the side filaments.

To understand this behaviour, let us return to equation (2). There are two key terms: the quasi-linear nonlinearity term $C_3\xi\frac{\partial^2\overline{\xi^2}}{\partial x_0^2}$ and the non-linear growth drive term $C_4(\xi^2 - \overline{\xi^2})$. Apart from the weak effect of viscosity, these are the only terms that couple in the y-direction, through the averaging of $\overline{\xi^2}$. This is therefore the dominant effect driving the interaction between the filaments. Later in time $\overline{\xi^2}$ is dominated by the contribution from the main filament peak as it is the largest

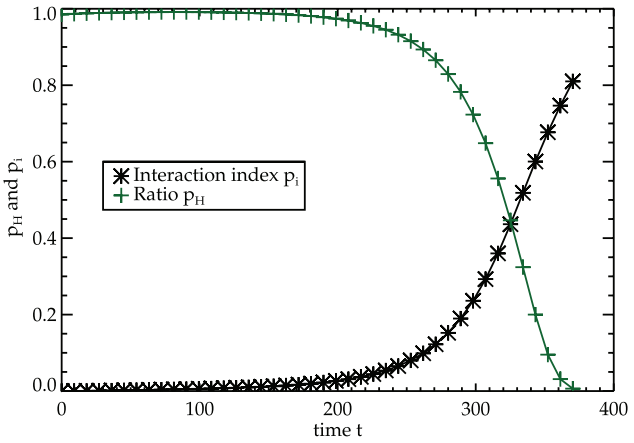

Figure 5. The ratio of the normalised height of the side filament to the main filament ($p_H = \frac{H_{sf}}{H_{mf}}$) versus time (green, +-Symbol) and the interaction-index for the main filament versus time ($p_i = \frac{\Delta\xi}{\xi_{n_1+n_2}}$) (black, *-Symbol).

contribution and there is little contribution from the side filaments. Therefore, for values of y_0 in the vicinity of the main filament peak, where $\xi^2 > \overline{\xi^2}$, this provides a drive. Elsewhere, $\xi^2 < \overline{\xi^2}$ so the term is negative which explains the reduced 'ground level' mentioned above. It also serves to damp the side filaments. The quasi-linear nonlinearity (C_3) is stabilising for both signs of ξ when $x = x_{max}$ where the second derivative of $\overline{\xi^2}$ is negative. It does however drive the disturbed region to broaden in x_0 since the second derivative of $\overline{\xi^2}$ is positive and therefore destabilising at the edges of the disturbed region.

To understand the physics, we return to our earlier statement that the $\overline{\xi^2}$ averaging is a consequence of the incompressibility of the plasma. As the main filament pushes up into the background plasma above it, it must displace that plasma. This causes a down-draft of plasma (represented by $\overline{\xi^2}$) that pushes back to either side of the main filament. This downwards flow of plasma suppresses the two side-filaments, particularly around $x_0 = x_{max}$, where the main filament is situated.

4. Conclusion

In summary, we have shown how the interaction between plasma filaments of slightly different amplitudes influences their evolution by solving the non-linear ballooning mode envelope equation with an Eulerian boundary condition. We have quantified this effect for a three filament system by introducing the interaction index p_i which characterises the difference between the two-mode simulation and the two independent single mode simulations. We demonstrated that the larger filament gains amplitude from the interaction with the smaller ones, which are suppressed. The larger filaments grow faster by devouring the smaller ones. It is expected therefore, that the filaments which first enter the non-linear regime will dominate the physics of plasma eruptions. This is in agreement with [14], where it is shown that if one starts with random small fluctuations, the filament with the biggest amplitude at

the transition from linear to non-linear grows fastest, and suppresses the other filaments. The qualitative behaviour of the main filament is similar to the single mode calculation, but it does grow faster as the finite time singularity is approached.

There is some experimental evidence for situations where the dynamics of explosive events are dominated by single filaments. One example is observations of high n ballooning modes in the precursor to disruptions on the TFTR tokamak [16]. As the disruption is approached the multiple filament structure appears to evolve into a single dominant filament. Another example is the small, so called type V ELMs which have been observed on the NSTX tokamak [17]. These involve fine-scale filaments that one would typically associate with higher toroidal mode numbers n. However, these ELMs only involve one or two filaments while one might expect $\sim n$ of them from linear theory. While experimental evidence suggests the dominant instability drive is current density rather than pure ballooning modes, it is possible that a similar mechanism to that identified here acts to limit the number of filaments.

Although our results are derived from a simple slab plasma model, it has the same features as more complex magnetic geometries, including tokamaks [5, 8]. We therefore believe the phenomenon of large filaments feeding off the smaller ones is a generic feature of ideal MHD. However, we note that the theory is only valid in the early non-linear stages of the evolution, and it requires that the dominant filaments will have time to have formed before the model becomes invalid. Also, we have not addressed the energy release mechanism. If this happens before the dominant filament 'eats' the smaller ones, the event will be a multi-filament event—otherwise only a few will dominate the eruptions. The complete process clearly involves an interaction of several complex mechanisms, so it is important to test these ideas in full, large scale simulations, close to marginal stability.

Acknowledgments

This work has been carried out within the framework of the EUROfusion Consortium and has received funding from the Euratom research and training programme 2014–2018 under grant agreement No 633053 and from the RCUK Energy Programme (grant number EP/I501045). The views and opinions expressed herein do not necessarily reflect those of the European Commission. Howard Wilson holds a Royal Society Wolfson Research Merit Award.

References

[1] Zohm H 1996 *Plasma Phys. Control. Fusion* **38** 105
[2] Connor J W, Hastie R J, Wilson H R and Miller R L 1998 *Phys. Plasmas* **5** 2687
[3] Leonard A W 2014 *Phys. Plasmas* **21** 090501
[4] Shibata K and Magara T 2011 *Living Rev. Sol. Phys.* **8** 6
[5] Hurricane O A, Fong B H and Cowley S C 1997 *Phys. Plasmas* **4** 3565–80
[6] Cowley S C and Artun M 1997 *Phys. Rep.* **283** 185–211
[7] Fong B H, Cowley S C and Hurricane O A 1999 *Phys. Rev. Lett.* **82** 4651–5
[8] Wilson H R and Cowley S C 2004 *Phys. Rev. Lett.* **92** 175006
[9] Connor J W, Hastie R J and Taylor J B 1979 *Proc. R. Soc.* **365** 1–17
[10] Ohsaki S, Shatashvili N L, Yoshida Z and Mahajan S M 2001 *Astrophys. J.* **559** L61
[11] Ohsaki S, Shatashvili N L, Yoshida Z and Mahajan S M 2002 *Astrophys. J.* **570** 395
[12] Cowley S C, Cowley B, Henneberg S A and Wilson H R 2015 *Proc. R. Soc.* A **471** 2180
[13] Kirk A *et al* 2006 *Phys. Rev. Lett.* **96** 185001
[14] Fong B H 2000 *PhD Thesis* Princeton University
[15] Landau L D and Lifshitz E M 2010 *Fluid Mechanics* 2nd edn (Amsterdam: Elsevier)
[16] Fredrickson E D *et al* 1996 *Phys. Plasmas* **3** 2620
[17] Maingi R *et al* 2006 *Phys. Plasmas* **13** 092510